Hindawi
Mathematical Problems in Engineering
Volume 2021, Article ID 6714418, 14 pages
https://doi.org/10.1155/2021/6714418

Research Article

Multistep Experimental Calibration of Mechanical Parameters for Modelling Multilayer Antishatter Safety Films in Structural Glass Protection

Chiara Bedon and Silvana Mattei

University of Trieste, Department of Engineering and Architecture, 34127 Trieste, Italy

Correspondence should be addressed to Chiara Bedon; chiara.bedon@dia.units.it

Received 19 September 2021; Accepted 9 November 2021; Published 23 November 2021

Academic Editor: Francesco Zammori

Glass material is largely used in buildings and facilities due to various motivations. Besides, glass still represents a vulnerable component for building occupants. Careful attention is required especially for glass elements that may be subjected to extreme design loads, such as impact, vibrations, etc. Among various approaches and techniques to prevent danger for people in case of glass breakage, multilayer antishatter safety films (ASFs) are commercially available for the retrofit of existing monolithic glass members. In the present research study, a multistep experimental program is presented to obtain the characterization of key input mechanical parameters that are required for the numerical analysis of glass elements protected by ASFs. Relevant characteristics are derived for the definition of an equivalent material and monolithic tape able to reproduce the ASF experimental outcomes. On the side of experiments, artificially aged specimens (healing process) are investigated. A major advantage is taken from small-scale peel and tensile tests on ASF samples, as well as Operational Modal Analysis (OMA) techniques for nondestructive vibration measurements on preliminary fractured specimens of ASF-bonded glass elements. Efficient Finite Element (FE) numerical models calibrated with the support of experimental data and Cohesive Zone Modelling (CZM) techniques are presented for discussion of comparative results, giving evidence of rather good estimates and possible extension of the multistep experimental procedure.

1. Introduction

Numerical modelling approaches, and in particular Finite Element (FE) techniques, are often used in research and design practice for a multitude of applications and scenarios. Among others, several studies have been spent in the years for the numerical analysis of structural performances in structural glass members and systems [1]. Glass in buildings still represents, after decades, a rather innovative constructional material and one of most vulnerable components. This requires careful consideration for structures that may be exposed to radiation or thermal ageing, abrasion phenomena [2], and extreme design actions such as impact, vibrations, etc. [3]. In the years, research studies have been also focused on breakage modelling and postbreakage parameter characterization for glass members [4–6].

Several terrorist attacks have shown that especially explosions could result in a massive failure of windows. Due to glass intrinsic fragility, its potential failure could consequently result in severe splinters that could seriously injure people (Figure 1(a)). When the use of safety laminated glass is not possible (i.e., to replace exiting monolithic elements), antishatter safety films (ASFs) represent one of the available techniques to improve the postcracked performance and possibly increase the expected protection levels (Figure 1(b)). Literature research reveals that several researches are available for glass components fitted with ASFs exposed to extreme loading [7–10]. In particular, Huang

(a) (b)

Figure 1: Glass window under hazard: (a) fracture pattern and (b) concept of ASFs.

et al. [11] investigated the influence of glass fragment retention films (FSFs), in the order from 4 to 14 mil in thickness, on the impact response by developing a nonlinear analytical model for the prediction of precrack impact strength.

Basic mechanical (and thermophysical) features of these ASFs are however directly responsible of the expected structural performance of bonded fractured glass elements [12, 13]. Moreover, peel adhesion and tensile test protocols generally provide the most representative parameters to assess the mechanical effectiveness of new or aged ASFs, as well as the basic features required to numerically account for the typical cohesive zone interaction near the crack tip during delamination from glass [14–18].

In the present study, the attention is focused on the experimental characterization and derivation of equivalent mechanical properties that can support a realistic analysis of glass elements bonded by ASFs. Based on different experimental techniques, more in detail, equivalent parameters are derived to provide useful background towards numerical simulations. A simplified monolithic thin tape reproducing the ASF characteristics and behaviour is in fact proposed to numerically replace the actual multilayer composition of typical commercial products. To this aim, the attention is focused on simple tape samples, classical peel adhesion specimens, but also Operational Modal Analysis (OMA) techniques on deliberately fractured ASF-bonded glass specimens. The discussion of comparative results shows that FE models can well capture most of the collected experimental findings. The present study can be thus efficiently extended to more detailed investigations on full-size samples and prototypes of ASF-bonded components, to assess their postbreakage performance and residual capacities, as well as to extend experimental approach to higher strain rates that are typical of glass components under impact.

2. Experimental Investigation

2.1. Multilayer Antishatter Safety Film. A commercial multilayer ASF with a constitutive stratification shown in Figure 2 was considered at the time of the experimental program.

Layers "1" and "2" are typically made of 0.22 mm polyethylene terephthalate (PET) amorphous and 0.11 mm PET semicrystalline, respectively, with a high degree of transparency and low permeability. Moreover, both layers are characterized by similar glass transition temperature (T_g), which is approximately equal to 80°C. The mechanical properties of ASFs mainly depend on the constituent polymeric layers and should be consequently separately characterized and calibrated. In this paper, otherwise, the multilayer composition is treated in the form of equivalent monolithic thin tape calibrated to experiments.

Pressure Sensitive Adhesive (PSA) is also known to create a temporary bond with the application of simple contact and slight pressure. This is possible thanks to a particular property (named *tack*), for which PSAs behave as liquids in case of low deformation rates and allow adapting perfectly to substrate surfaces. Moreover, a removable release liner protects the PSA and prevents it from unwanted sticking. As this part is removed before the installation of the ASF onto the glass element, it has no influence whatsoever on the (mechanical) behaviour of glass itself and is therefore disregarded in the herein summarized investigation.

2.2. Influencing Parameters for Mechanical Characterization of PET. Different parameters can typically affect the mechanical properties of laminated glass (i.e., interlayer foils), but also ASF properties. Among others, for example, it is known that temperature (but also humidity, loading time, and strain rate, etc.) can have severe degradation effects on the actual mechanical capacities and thus on the structural performance of bonded elements [19–22].

Regarding ASFs for structural glass applications, the influence of temperature on the mechanical behaviour of PET, in particular, has been demonstrated by several literature studies [23, 24]. In particular, the variation of elastic modulus with temperature is typical of a viscoelastic material. Arkhireyeva and Hashemi [25] analysed the thermal degradation of an amorphous PET film within the 23–70°C temperature range. Although the explored ageing temperature can be seen as below the glass transition temperature

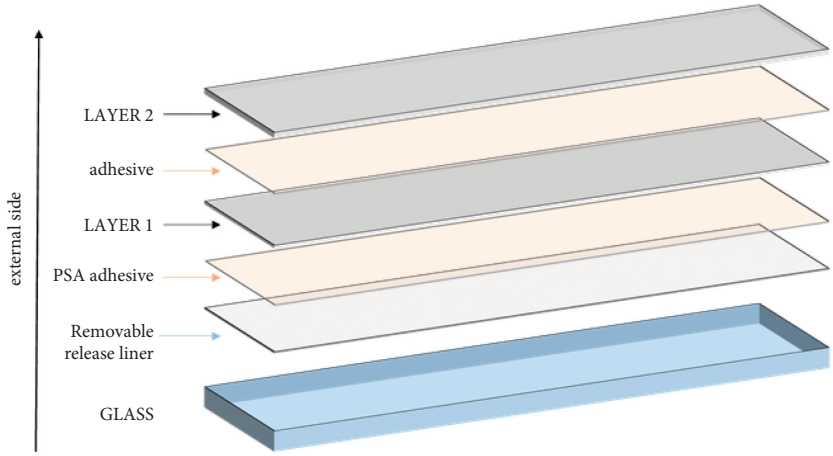

Figure 2: Stratification detail of the examined multilayer ASF.

($T_g \approx 80^{\circ}$C), the reduction of tensile properties can be perceived clearly. A typical trend of experimental data discussed in [25] is emphasized with fitting curves in Figure 3.

2.3. Preparation of ASF-Bonded Samples. The experimental tests involved a number of 5 small-scale specimens, with fixed nominal geometric characteristics and pretest phases. In order to account for ageing effects, based also on Figure 3, a preliminary treatment at a healing temperature of 50°C for 72 hours was taken into account for all the samples.

The strips were compression-moulded on a rigid glass substrate (annealed glass) with 100×40 mm nominal dimension (6 mm in thickness). High pressure was applied, in order to be perfectly adherent the ASF strips with glass. All the adhesions have been realized placing much care in the superimposition of the ASF, so as to avoid the creation of bubbles and superficial folding. To minimize the influence of little impurities or inclusions, the glass surface was also treated and the protection layer was quickly peeled off. Then, a pressure was manually applied to the ASF to remove any residual heterogeneity to make the adhesion as much homogeneous as possible. The so-assembled samples were used for peel tests and vibration tests.

The aforementioned technique follows a practice procedure named dry lamination. To obtain a dry film, a layer of adhesive is applied on the film that at the time of lamination can be brought to light by heated grille. Dry films offer a number of advantages in different respects compared to wet films: cheaper laminating machines, faster start-ups, no glue assembly, ready-to-use couplings for subsequent processing in less time than wet films, and less environmental impact. The critical step is the thorough cleaning of the glass surface, on which depends the efficiency of adhesive bond. For these systems the adhesion force achieved between the interfaces develops in a short time. The goodness of an adhesive depends not only on its ability to mate to the surface with a low pressure and small contact time but also on its ability to form a fibrillar structure when detached from the substrate. This aspect is also strictly connected to the cohesive behaviour leading to a modification of peel-off force value [26] since the process zone is defined as the region from the last detached fibril to the critical point where the fibrillation starts, which is the contact point between the adhesive tape and the glass substrate.

3. Experimental Methods

Different experimental methods were taken into account in the multistep approach, so as to detect the input mechanical properties of typical ASFs for possible numerical applications in structural glass context. The experimental program was carried out in 2021 at University of Trieste (Italy), Department of Engineering and Architecture, in the form of quasistatic peel tests on small-scale samples of ASF-bonded glass elements, quasistatic tensile tests (on tape samples only), and low-velocity, nondestructive vibration tests on prefractured small-scale samples of ASF-bonded glass fragments.

3.1. Peel Tests. The experiments were conducted with a standard tensile machine to control peel rate, by employing a short initial peel arm as shown in Figure 4. The used experimental setup was characterized by a nonconstant peel angle θ and was able to rapidly change during the entire loading process [27]. The specimens were in fact installed on the machine through 4 bolts (2 per side), in order to guarantee a fixed connection and avoid any relative movement of support during the tests.

The ASF was then folded and stuck in the machine clamp. The width and the thickness of the tape backing were measured in 25 mm and 35 μm, respectively. The reference test was carried out in displacement control, with a speed of 25.4 mm/min. No external equipment was used to measure displacements, and thus the constitutive diagrams were derived from machine data only. Under the imposed vertical displacement, the experiments were stopped once the tape was completely detached from glass support.

3.2. Tensile Tests. In parallel to peel experiments, a tensile test protocol was carried out using a Shimadzu universal testing machine. This test method is generally adopted for plastics in the form of thin sheeting, including film layers with a thickness less than 1 mm.

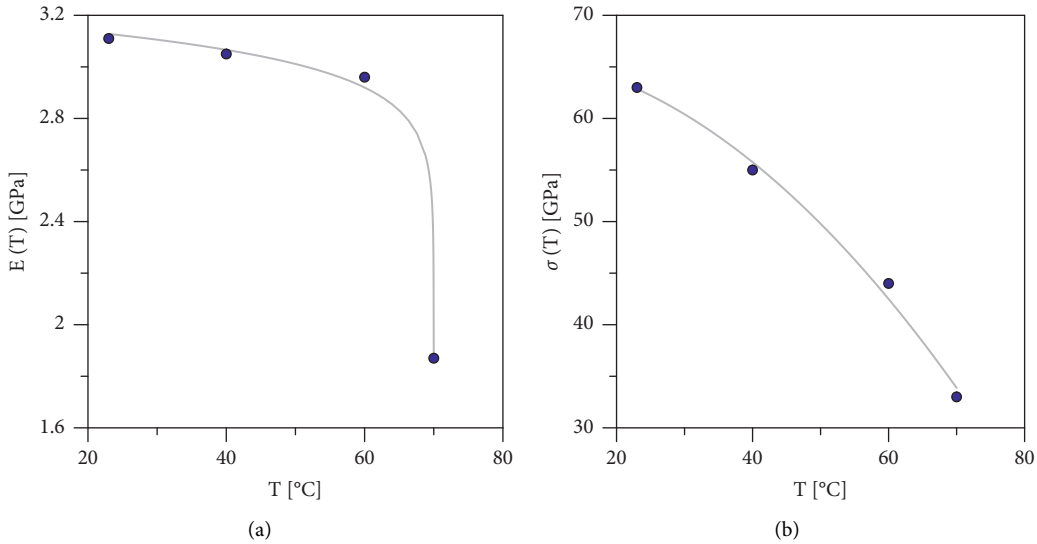

Figure 3: Sensitivity of PET film mechanical parameters to temperature (adapted from [25]): variation of (a) modulus of elasticity and (b) strength as a function of temperature.

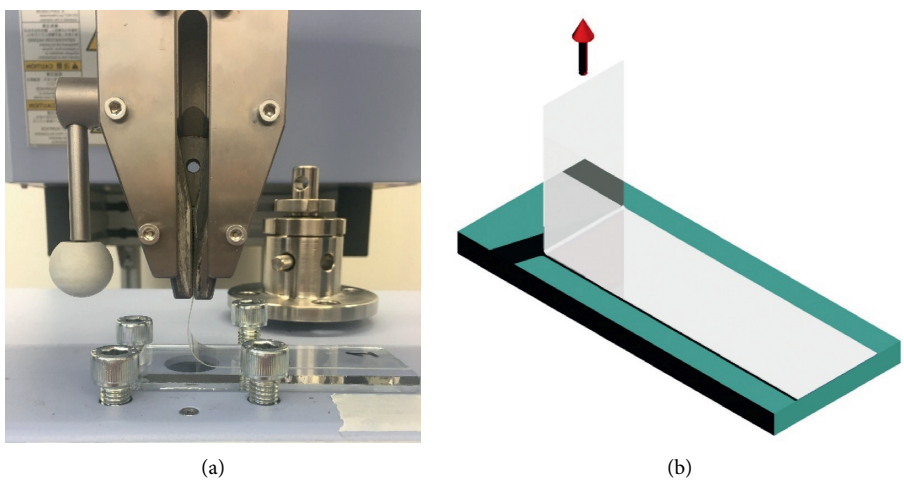

Figure 4: Peel test: (a) setup detail and (b) schematic model.

Pure tensile tests were conducted on ASF tapes to determine the corresponding quasistatic elastic modulus E. This step was carried out to support the interpretation of peel test measurements and specifically to encompass the extensibility in the ASF portion not in adherence with the glass substrate (Figure 4). A number of 5 rectangular shaped specimens were sized in 350×25 mm (Figures 5(a) and 5(b)). The setup in Figure 5(c) was designed according to ASTM D882-02 provisions [28]. The multilayer ASF tape was preliminary treated with acetone, in order to remove the adhesive part schematized in Figure 2. Moreover, an adhesive layer (RS PRO Industrial Grade Adhesive 132633) was applied on the final length (50 mm) on both sides of each specimen. This can be noted in Figures 5(a) and 5(b). The adhesive layer was left hardening on the PET film to create a nonslippery surface in correspondence of machine grips. The tests were conducted with a constant displacement rate of grip separation (25 mm/min), until failure of each tape.

3.3. Vibration Tests. At a final stage of the experimental study, nondestructive vibration experiments were carried out on small-scale samples of ASF-bonded glass elements. As a key feature of vibration tests, the glass specimens from Section 3.2 were reused and deliberately fractured before the execution of dynamic experiments. A steel hammer was used to crack glass, so that the ASF could keep together major glass fragments as in Figure 6(a). The use of annealed glass, in this regard, was privileged to other glass types, in order to facilitate the propagation of few major cracks and fragments in place of a large number of small fragments as for tempered glass elements.

The vibration experiments were carried out under a simple support configuration (Figure 6(b)). The schematic drawing gives evidence of the initial precracked condition of ASF-bonded samples, as well as the expected behaviour under imposed vibrations. For the reference setup, glass portions were made free to bend under positive bending

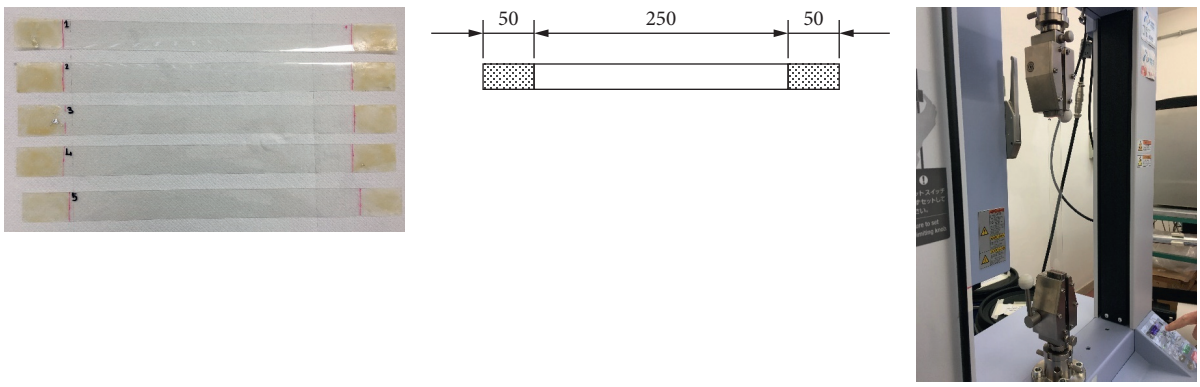

(a) (b) (c)

Figure 5: Tensile tests: (a) specimens and (b) nominal dimensions (in mm), with (c) loading stage.

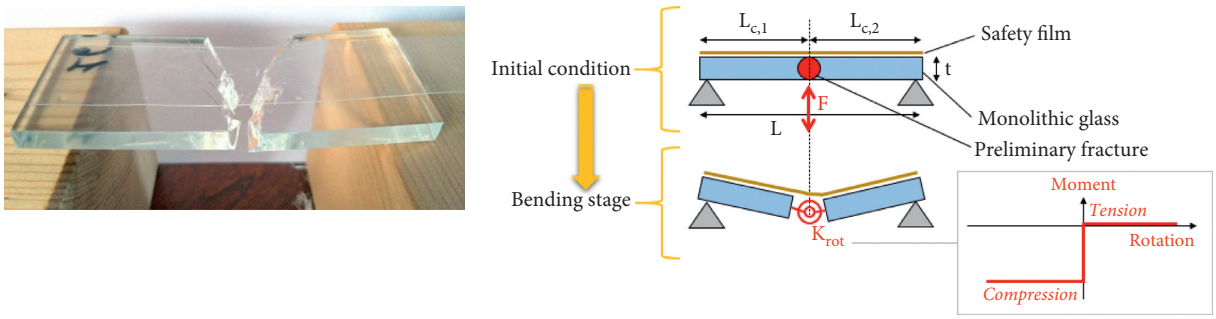

(a) (b)

Figure 6: Vibration tests on fractured sample: (a) typical specimen and (b) schematic setup.

moment, while possible mechanical interaction (if any) could occur under negative bending moment only. For the presently investigated specimens, in particular, the attention was focused on the fracture of glass fragments that could avoid any kind of contact for glass elements (i.e., null mechanical interaction and postbreakage stiffness in tension and compression).

The vibration response of such a kind of fractured specimens was carried out with the support of a Micro-electromechanical Systems (MEMS) accelerometer that was connected to each sample [29]. The measurement of triaxial acceleration records for the specimens under low-velocity vibrations was in fact combined with dynamic identification and classical OMA techniques that are typical of structural health monitoring applications for buildings but can be successfully adopted to address structural glass issues [30, 31], even for postbreakage considerations [32]. For the present investigation, the goal was specifically focused on the inverse characterization of the mechanical properties of bonding ASFs under vibrations, as it is in a typical postevent scenario.

4. Experimental Results

4.1. Peel Tests and Influence Analysis of Variable Peel Angle θ. Figure 7 shows the typical measured peel force, as a function of the imposed vertical displacement. As the adhesive is peeled, it can be seen in Figure 7 that the peel force P increases until it levels off at a roughly steady-state value. This is the steady-state region, where the focus of the present investigation was primarily directed. The P amplitude for each test in the steady-state region was taken as an average of measured values (in general, past 25 mm). It is worth to note that this aspect is less recognizable than in case of a constant θ angle for peel tests, where equilibrium is reached, due to the continuously varying tip velocity as a function of θ, while the imposed velocity remains constant.

By considering that the edge of the ASF tape engaged in the grip was vertically displaced to propagate peeling phenomenon, the force value measured by the load cell was not representative of the exact definition of peel force. To obtain the correct peel force value, a further intermediate elaboration was made necessary, so as to assess the evolution of θ during each experiment.

For inextensible films, the peel strength is generally controlled by peel angle θ and adhesion energy, which can be evaluated based on Kendall model [33]. By considering a fixed reference system with horizontal x-axis in the direction of peeling progress and vertical y-axis for imposed displacements (see Figure 8), the instantaneous peel arm length can be expressed as $l = l_0 + d$, where l_0 is initial peel arm length and d is the imposed displacement.

The corresponding peel angle θ can be thus evaluated as

$$\theta = \cos^{-1}\left(\frac{l_0 \cos\theta_0 + d}{l_0 + d}\right). \quad (1)$$

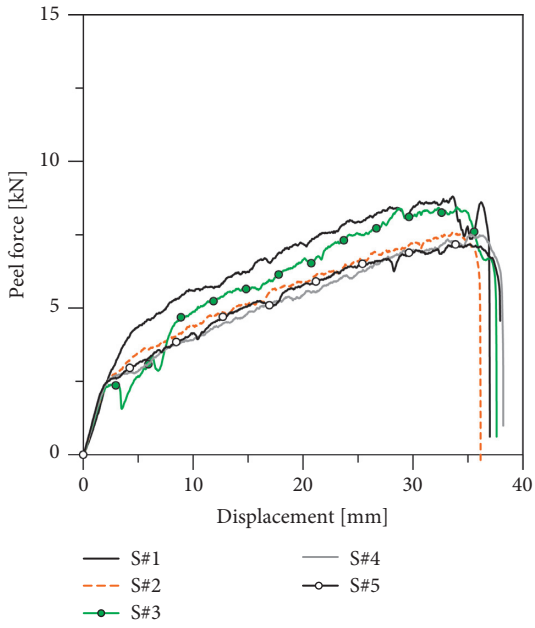

Figure 7: Experimental peel curves.

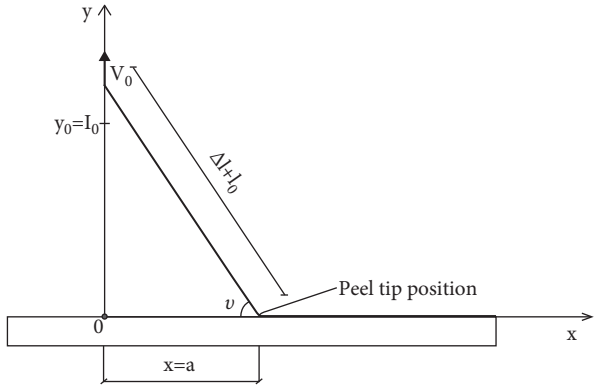

Figure 8: Geometric configuration of peeling process.

In addition, an elastic term in the film deformation during the test may be considered. From the geometrical system in Figure 8, this term can be calculated as

$$(l_0 + \Delta l)^2 = y^2 + d^2, \tag{2}$$

where Δl considers the increase of peel arm length as the sum of two terms, the elastic deformation of the tape and the peeling advancing under the imposed displacement. Equation (2) can be hence reformulated as

$$\left(l_0 + \left(\frac{y_i - y_0}{\text{sen}\theta_i}\right)\right)^2 = (y_0 + y_i)^2 + d_i^2. \tag{3}$$

The above observations lead to the correct assessment of peel force P based on the force component P_v (computed from the load cell data), that is, $P = P_v/\text{sen}\theta$. Note that a higher value of P was generally observed due to the decrease of peel angle (Figure 9).

The peel test assessment as a fracture mechanics problem was first introduced by Kinloch et al. [34]. An adhesive fracture energy term (G) was introduced as a contribution which can be determined by taking into account the energy dissipation due to plastic or viscoelastic bending and tensile deformations of the peeling arm. The approach in [33] describes the energy per unit area of peel propagation as

$$G = \frac{1}{b}\left(\frac{dU_{\text{ext}}}{da} - \frac{dU_s}{da} - \frac{dU_{dt}}{da} - \frac{dU_{db}}{da}\right), \tag{4}$$

and is based on energy-type criterion to express the fracture energy in a surface creation (da, b its width) as a conversion of the external work by external forces (U_{ext}); the available energy stored in the specimen (U_s); the dissipated energy during tensile (elongation energy U_{dt}) or bending deformations (bending energy U_{db}).

The presence of peel angle in each term of equation (4) leads to discretizing the formulation in order to compute a preliminary value of G, so as to derive a tentative input value for the numerical calibration in Section 5.

4.2. Tensile Tests. The quasistatic elastic modulus was derived from the slope of linear branch for the collected stress-strain curves of tested tapes, as in Figure 10. After TOE compensation, the average calculated value resulted in $E_{\text{film}} = 3.31$ GPa (±139 MPa, the standard deviation), which was also found to agree with values of literature (i.e., Figure 2 and others). Therefore, the elastic-plastic material model of the film was characterized by another three parameters which are generally reported in datasheets of commercial products and, namely, represented by elongation at break, tensile strength, and yield strength. For practical building applications, various films are available to retrofit glass elements. For comparative analysis of experimental outputs from the tensile tests, Table 1 reports some nominal mechanical parameters for selected products.

4.3. Vibration Tests. Following the simply supported setup of cracked samples as in Figure 6, the typical postprocessing stage of raw data was carried out on experimental acceleration time histories in accordance with Figure 11(a). A number of around 30 test repetitions were carried out in total, so as to capture vibration records for all the tested samples and under a different level of acceleration amplitudes. Based on the size of small-scale samples, the parametric experimental analysis was focused on the range of $a = \lceil 0\text{–}1.2 \rceil\ g$ for the vertical component of accelerations. The analysis of records was in fact dedicated to the vertical acquisitions only. Based on the available MEMS sensor and the collected measurements, the dynamic parameters of samples were estimated by means of the Structural Modal Identification Toolsuite software (SMIT [38]). The ERA-OKID-OO approach [39, 40] was preferred to other techniques, because it is able to offer more stable identification results.

As a final result, fundamental vibration frequencies of simply supported cracked glass fragments bonded by anti-shatter safety films were separately collected and compared as a function of maximum acceleration peak. The typical result is summarized in Figure 11(b) for grouped samples.

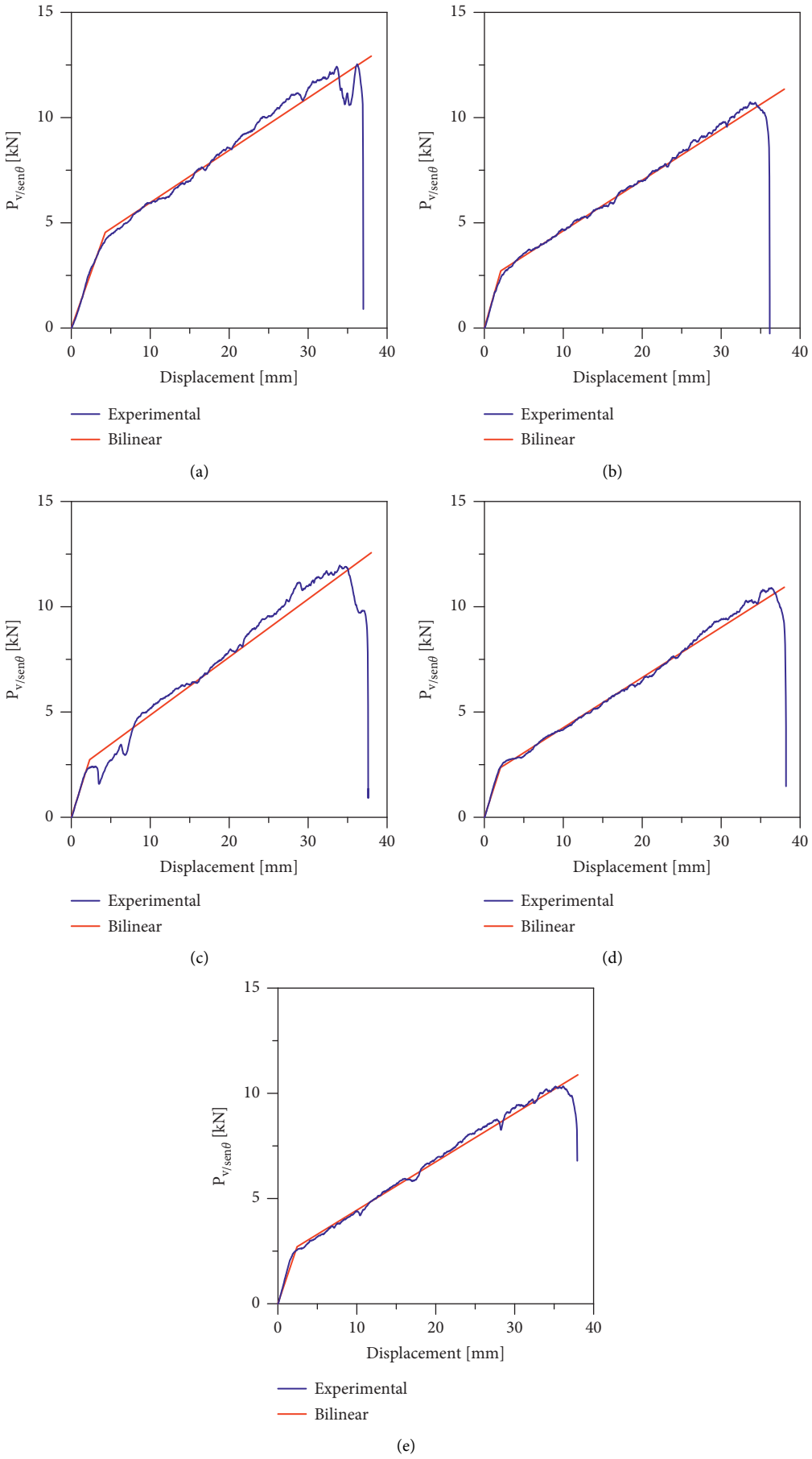

Figure 9: Experimental peel curves and corresponding bilinear curves, as corrected by θ variability. (a) *S*#1. (b) *S*#2. (c) *S*#3. (d) *S*#4. (e) *S*#5.

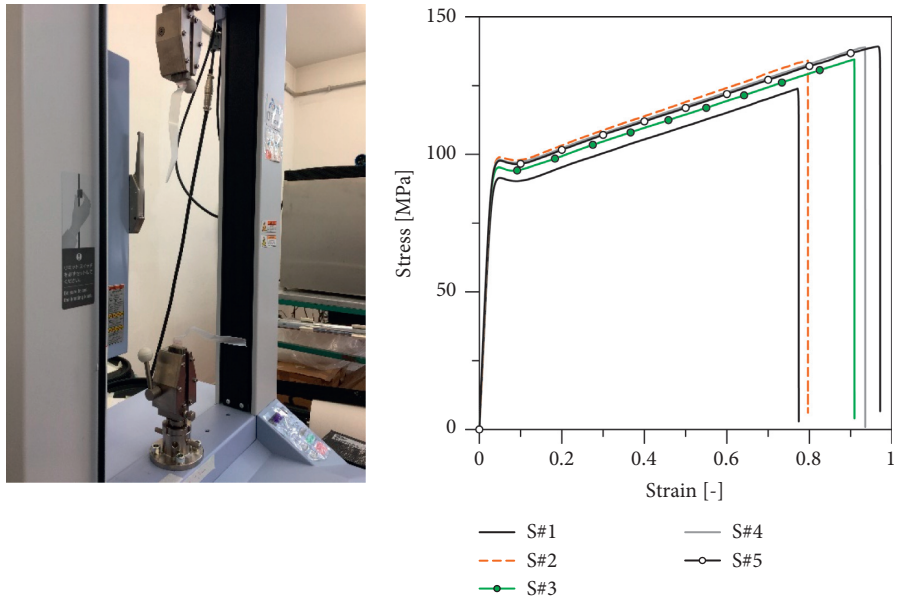

Figure 10: Tensile tests: (a) failure and (b) stress-strain curves for tested samples.

Table 1: Comparison of mechanical properties for the examined PET film and selected commercial products.

	Elongation (%)	Tensile strength (MPa)	Yield strength (MPa)
Currently tested PET film	88 ± 8.7	134 ± 6.2	96 ± 3.0
3M–ultra S800 [35]	>100	207	103
Solarcheck–14 mil clear [36]	>100	211	—
Bekaert specialty film [37]	>100	200	100

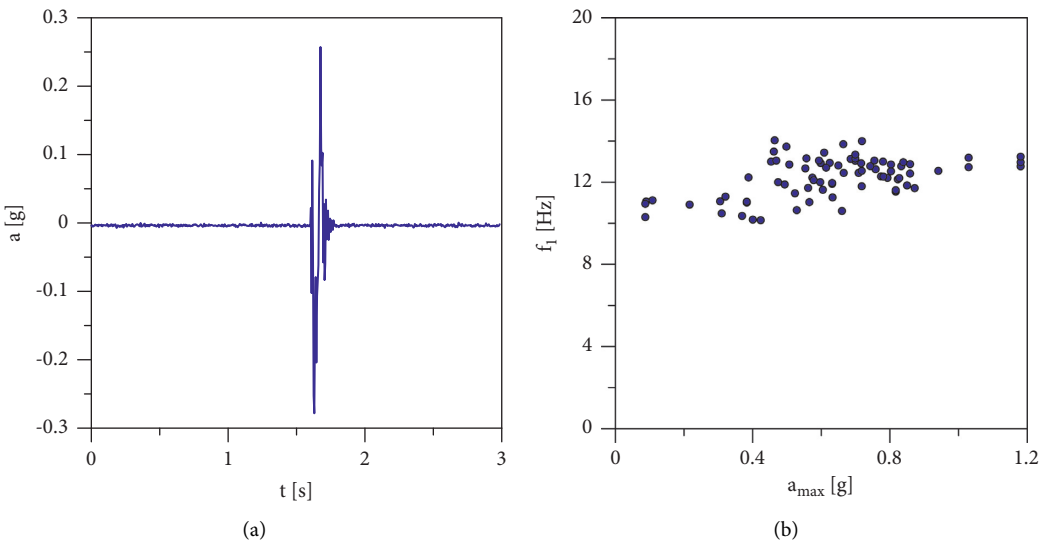

Figure 11: Vibration experiments on fractured samples: (a) typical acceleration records (vertical component) and (b) calculated fundamental frequencies as a function of the imposed acceleration peaks.

5. Numerical Modelling of Peel Simulations

5.1. Model Assembly. A Finite Element (FE) numerical model was developed in ABAQUS/Explicit for the tested peel specimens [41]. The reference model was used to assess the adhesion energy and to develop a consistent cohesive zone law for the specific protective film in a peeling configuration. The cohesive zone law is usually developed in computation fracture mechanics for describing the stress state around the crack tip. In the present study, the cohesive

zone model (CZM) formulation from ABAQUS library was used in order to investigate and properly reproduce the experimental setup and outcomes [42].

The modelling strategy was characterized by a preliminary simulation to place the thin ASF in the exact test configuration, that is, with an initial peel angle of 90 degrees. The numerical model (i.e., Figure 12(a)) consisted of 3D solid elements with 8 nodes (C3D8R type) representative of glass and the portion of ASF which is initially in adherence to the rigid substrate. At the same time, the free length of peel arm was modelled as 4-node shell elements (S4R type), so as to reduce the computational effort of simulations. The two parts of the tape were properly constrained with a *shell-to-solid* connection, so as to simulate the continuity in the element. Finally, the *encastre* boundary condition (degrees of freedom 1, 2, 3, 4, 5, 6 = 0) at the bottom of the glass element was used.

5.2. Material Properties and Interactions. Regarding the characterization of materials, an ideal linear elastic constitutive law was used for annealed glass. Such a choice was justified by the contribution of glass as a rigid substrate only for the examined setup. Furthermore, it was not expected to interfere in the delamination process, due to the low levels of loading. The modulus of elasticity, Poisson ratio, and density for glass were set, respectively, in 70 GPa, 0.23, and 2500 kg/m^3 (Table 2). The input parameters included the material properties of the ASF tape, which were preliminary derived as results of tensile tests in Section 3. Based on subsequent considerations and comparative analysis, the modulus was fitted to $E_{\text{film}} = 3.2$ GPa, with 0.35 the corresponding Poisson ratio and 1350 kg/m^3 material density, as reported in Table 2.

Special care was finally spent for the CZM characterization. The adhesive layer was modelled as a *surface-to-surface* interaction characterized by a linear cohesive law between glass and PET film. In particular, the considered model in a mode-I fracture problem can be referred to a traction-separation law, in which in correspondence of crack tip the delamination occurs when the separation reaches a critical value (δ_0). A schematic representation of the typical triangular CZM is defined as a function of two key parameters in Figure 12(b), namely, peak stress (t_0) and critical crack tip opening displacement (δ_0), or fracture energy equivalent to the area under the bilinear curve.

Moreover, experimental data from peeling tests were used to assess and calibrate the CZM input features: adhesion fracture energy G and three components of nominal peak stresses (t_n, t_s, and t_t) for the cohesive interface. The CZM simulates the elastic behaviour up to the traction strength and subsequent softening up to separation failure (δ_t). Elasticity is then defined by a constitutive matrix where the stiffness parameters for the present analysis were derived from the elastic ASF moduli (E_{film} and G_{film}), by considering isotropic adhesive behaviour in the s and t shear directions:

$$t = K\varepsilon = \begin{bmatrix} K_{nn} & 0 & 0 \\ 0 & K_{ss} & 0 \\ 0 & 0 & K_{tt} \end{bmatrix} \begin{Bmatrix} \varepsilon_n \\ \varepsilon_s \\ \varepsilon_t \end{Bmatrix} = \begin{bmatrix} \dfrac{E_{a\,dh}}{t_{a\,dh}} & 0 & 0 \\ 0 & \dfrac{G_{a\,dh}}{t_{a\,dh}} & 0 \\ 0 & 0 & \dfrac{G_{a\,dh}}{t_{a\,dh}} \end{bmatrix} \begin{Bmatrix} \varepsilon_n \\ \varepsilon_s \\ \varepsilon_t \end{Bmatrix}. \tag{5}$$

The peak and softening branch in Figure 12(b) are commonly described in ABAQUS in the form of damage "initiation" and "evolution" parameters. The former can be specified by different criteria which provide threshold stress value as a combination of three components. In the present study, the maximum nominal stress (MAXS) criterion was considered for damage initiation (with $t_n^0 = t_s^0 = t_t^0$):

$$\max\left\{\frac{t_n}{t_n^0}; \frac{t_s}{t_s^0}; \frac{t_t}{t_t^0}\right\} = 1. \tag{6}$$

On the basis that one of the most commonly used forms for that is a power law, the damage evolution criterion contemplates a linear softening (i.e., $n = 1$) as a function of G. To monitor the increase of peel tip position, an overall value of scalar damage variable (D) was taken into account during the numerical simulations, which is also known as CSDMG in ABAQUS library. After the initiation of damage, the D-value monotonically increases from 0 to 1, representative of undamaged and fully damaged material, respectively.

5.3. Comparison of Numerical and Experimental Data. The peel test setup was numerically reproduced in the form of dynamic simulations. Quasistatic vertical displacement was imposed in ABAQUS at the end of the tape backing, by monitoring the energy balance of each FE model. Based on a numerical iterative process (with G set as the only variable parameter of the reference FE model), each sample was analysed to detect the best fitting with experimental measurements. The output of simulations was arranged in the form of peel force as a function of the imposed vertical displacement and thus compared with the experimental peeling curves.

The collected numerical curves showed a general trend, on average terms, able to reflect well the laboratory experience (Figure 13). The scatter between the experimental and numerical curves was mainly justified by minor issues related to the preparation of samples, rather than to a poor precision of the models. In the comparative chart of Figure 13(a), for example, it is evident that the numerical curve does not match the initial branch of the experimental one in a coherent way. Such a trend can be associated with the experimental setup procedure (90-degree fold) and to the consequent (possible) premature detachment of the ASF portion corresponding to peel tip position, which is not

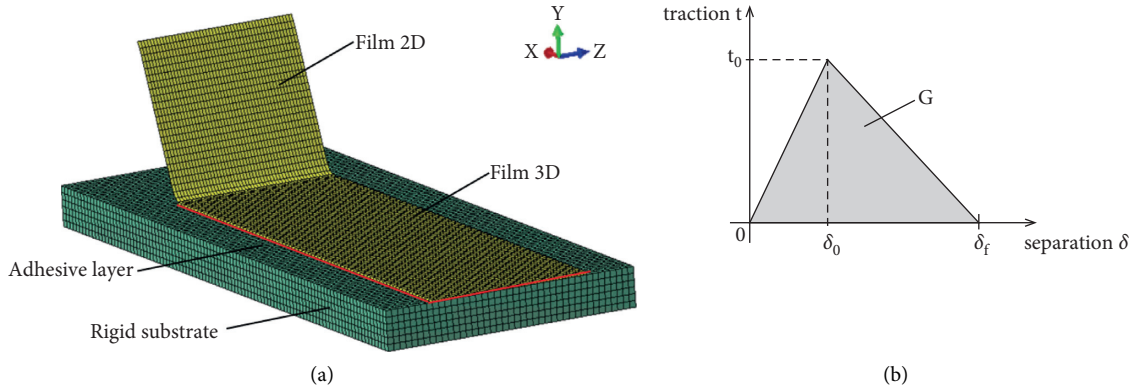

Figure 12: (a) Reference FE numerical model for peel (ABAQUS) and (b) detail of traction-separation law in case of linear softening for damage evolution.

Table 2: Input material properties.

	γ (kg/m^3)	E (GPa)	ν (-)
Glass	2500	70	0.23
ASF	1350	3.2	0.35

captured on the numerical side. In any case, rather close correlation can be noticed in Figure 13 for the tested samples.

As a further confirmation of modelling strategy, it is possible to see in Figure 14 that the outputs of experimentally and numerically derived values of fracture energy G are similar for all the samples, with a mean percentage scatter in the order of ≈26%. In terms of dispersions of datasets with respect to the mean, the sample standard deviation parameter can be used to make estimates about spread for variability. For the present study, this was calculated in approximately $\sigma_{exp} = \pm 10$ J/m^2 and $\sigma_{num} = \pm 11$ J/m^2. Such a finding can also be noted in Figure 14, where the different set of outputs shows a similar dispersion statistic.

6. Numerical Modelling of Vibration Tests

The FE model for frequency estimates was still developed in ABAQUS/Standard for all the tested specimens, but with the introduction of some geometrical simplifications. The reference model included in fact two glass portions representative of actual fragments (based on local measurement of samples) and the nominal size of bonding film. Shell elements (S4R type) and brick elements (C3D8R type), respectively, were used for glass and ASF parts, with linear elastic material properties. Input material properties were defined as for the peel simulations in Section 5 (see Table 2). The difference of present analyses was represented by a fully rigid bonding of ASF shell elements with glass brick fragments (*tie* constraint), in place of CZM surface interactions. Equivalent nodal restraints were finally distributed at the end/bottom edges of brick glass fragments, so as to reproduce the experimental setup in Figure 6 (linear supports). Linear modal analyses were carried out to estimate the fundamental frequency and modal shape of fractured simply supported ASF-boned specimens.

From the numerical analysis, a typical modal shape of beam in bending was captured for most of them. An example can be seen in Figure 15(a). The average fundamental frequency was numerically estimated in $f_1 = 14.51$ Hz, which was found to represent an upper bound for the available experimental data (Figure 15(b)). On one side, such a finding suggests the high sensitivity of vibration parameters to possible localized delamination (i.e., in the region of fracture, where maximum deflections were imposed to samples), which was not accounted by numerical simulations. On the other side, the numerical outcomes can also suggest a sensitivity of ASF tape stiffness to the imposed acceleration amplitudes.

In this regard, Figure 15(c) shows the calculated trend of numerical fundamental frequency by varying the modulus of elasticity of the tape. The more the ASF tape is stiff, the higher the corresponding frequency of composite sample is, as expected. The reference input modulus from the quasistatic experiments is also emphasized in the graph. It is worth to note in Figures 15(b) and 15(c) that the top frequency value from experiments can be experimentally fitted by a tape modulus of $E_{film} \approx 2.9$ GPa, which is lower than the quasistatic estimate and could suggest the presence of some local delamination in the region of glass fracture. At the same time, the so-calculated modulus is in correlation with the dynamic elastic modulus experimentally derived in [12] for similar ASF products. In this context, the proposed modelling approach can capture approximately only the theoretical dynamic behaviour of fractured glass samples and encourages a more detailed experimental analysis in this direction.

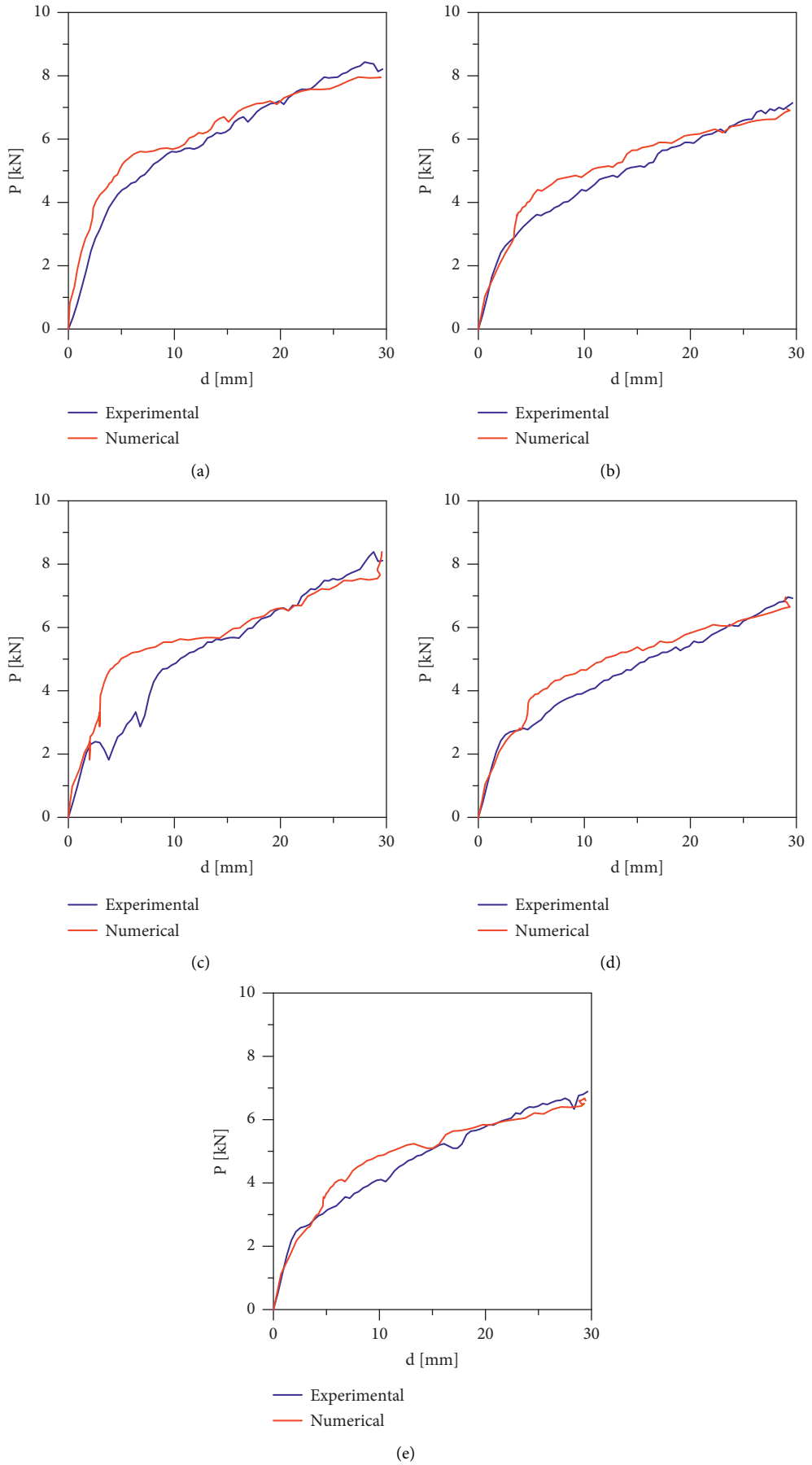

Figure 13: Comparison between experimental and numerical peel curves. (a) *S*#1. (b) *S*#2. (c) *S*#3. (d) *S*#4. (e) *S*#5.

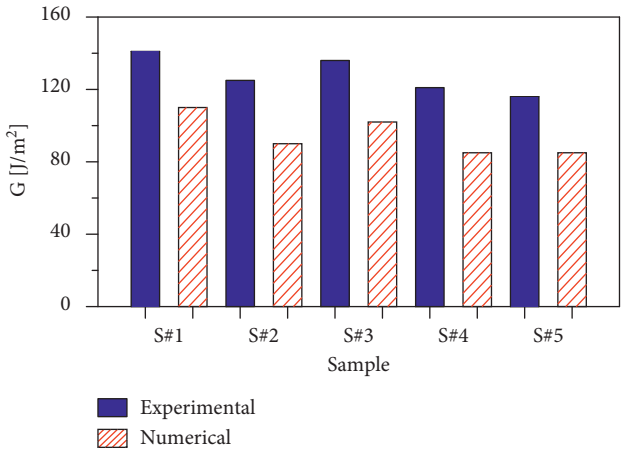

Figure 14: Comparison of fracture energy estimates from peel experiments and simulations.

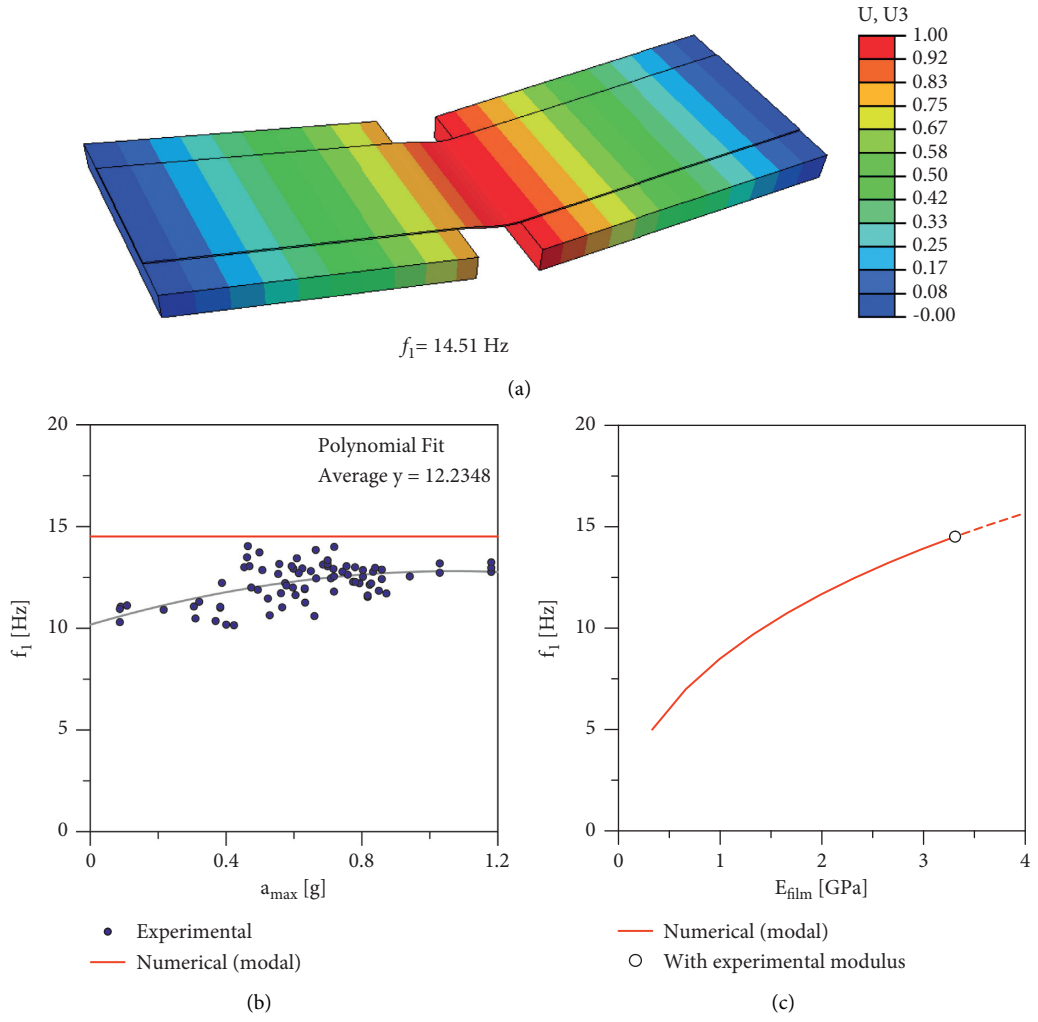

Figure 15: Vibration analysis: (a) example of fundamental vibration frequency and shape for simply supported fractured ASF-bonded glass sample (ABAQUS) and (b) comparison of experimental frequencies with modal analysis, with (c) variation of numerical frequency with E_{film}.

7. Conclusions

The use of structural glass in buildings is generally characterized by several advantages but also associated with high vulnerability which depends on the fragile material behaviour. Special design attention is thus required for glass members that are expected to suffer from severe and/or exceptional design actions.

In the context of retrofit interventions, one of commercially available techniques to improve the protection level for glass components is represented by the application of multilayer antishatter safety films (ASFs) that are expected to minimize possible shards and splinters against people, in the event of breakage.

In this paper, the attention was focused on the mechanical characterization of a selected commercial multilayer ASF and on the experimental derivation of basic mechanical parameters to support an efficient Finite Element (FE) numerical analysis of ASF-bonded glass elements. In doing so, a major advantage was taken from the use of conventional peel adhesion and tensile test protocols but also from the adaptation of Operational Modal Analysis (OMA) techniques for dynamic identification to deliberately fractured ASF-bonded glass specimens.

Artificially aged specimens (healing process) were investigated. A simplified, equivalent monolithic tape calibrated to experimental outcomes was proposed for a realistic numerical characterization approach. The comparative results, as shown, proved that the so calibrated numerical models and related simulations can capture most of the experimental observations. In this regard, the present research outcomes suggest the development of more extended investigations on full-scale size samples and prototypes of ASF-bonded glass components, so as to assess their postbreakage residual capacities under different strain rates and impact conditions.

Data Availability

The data supporting the research study will be shared upon request.

Conflicts of Interest

The authors declare that they have no conflicts of interest.

Acknowledgments

Prof. Chiara Schmid and Dr. Luca Cozzarini are gratefully acknowledged for the support during the experimental investigation carried out at University of Trieste, Department of Engineering and Architecture (Italy). This research study was financially supported by University of Trieste within the "SHARBAR" project (Microgrants 2020 program, Principal Investigator C. Bedon).

References

[1] M. Larcher, M. Arrigoni, C. Bedon et al., "Design of blast-loaded glazing windows and facades: a review of essential requirements towards standardization," *Advances in Civil Engineering*, vol. 2016, Article ID 2604232, 14 pages, 2016.

[2] C. Ferretti, P. Ganugi, G. Pisano, and F. Zammori, "Abraded glass strength: an ad hoc fitting protocol based on the change of variable theorem," *Mathematical Problems in Engineering*, vol. 2020, Article ID 8519426, 12 pages, 2020.

[3] C. Bedon, X. Zhang, F. Santos et al., "Performance of structural glass facades under extreme loads - design methods, existing research, current issues and trends," *Construction and Building Materials*, vol. 163, pp. 921–937, 2018.

[4] M. Vocialta, M. Corrado, and J.-F. Molinari, "Numerical analysis of fragmentation in tempered glass with parallel dynamic insertion of cohesive elements," *Engineering Fracture Mechanics*, vol. 188, pp. 448–469, 2018.

[5] C. Alter, S. Kolling, and J. Schneider, "An enhanced non-local failure criterion for laminated glass under low velocity impact," *International Journal of Impact Engineering*, vol. 109, pp. 342–353, 2017.

[6] L. Galuppi and G. Royer-Carfagni, "The post-breakage response of laminated heat-treated glass under in plane and out of plane loading," *Composites Part B: Engineering*, vol. 147, pp. 227–239, 2018.

[7] S. Van Dam, J. Pelfrene, S. De Pauw, and W. Van Paepegem, "Experimental study on the dynamic behaviour of glass fitted with safety window film with a small-scale drop weight set-up," *International Journal of Impact Engineering*, vol. 73, pp. 101–111, 2014.

[8] T. Kojima, M. Suzuki, and M. Notomi, "Numerical simulation on dynamic fracture of glass plate fitted with polymeric film," *Advanced Materials Research*, vol. 1166, pp. 57–64, 2021.

[9] S. D. Pauw, *Experimental and numerical study of impact on window glass fitted with safety window film*, PhD Thesis, Ghent University, Ghent, Belgium, 2010.

[10] K. C. A. Kook Chan Ahn, "Impact response of the film mechanical properties of the coated glass plate," *International Journal of Mechanical and Production Engineering Research and Development*, vol. 9, no. 2, pp. 499–506, 2019.

[11] X.-H. Huang, X. Wang, J. Yang, Z. Pan, F. Wang, and I. Azim, "Nonlinear analytical study of structural laminated glass under hard body impact in the pre-crack stage," *Thin-Walled Structures*, vol. 167, Article ID 108137, 2021.

[12] D. Papán, Z. Papánová, and L. Figuli, "Dynamic and static tests of the safety foil for windows for composite glass interaction," *MATEC Web of Conferences*, vol. 313, Article ID 00029, 2020.

[13] L. Figuli, D. Papan, Z. Papanova, and C. Bedon, "Experimental mechanical analysis of traditional in-service glass windows subjected to dynamic tests and hard body impact," *Smart Structures and Systems*, vol. 27, no. 2, pp. 365–378, 2021.

[14] P. Rahulkumar, A. Jagota, S. J. Bennison, and S. Saigal, "Cohesive element modeling of viscoelastic fracture: application to peel testing of polymers," *International Journal of Solids and Structures*, vol. 37, no. 13, pp. 1873–1897, 2000.

[15] A. N. Raegen, K. Dalnoki-Veress, K.-T. Wan, and R. A. L. Jones, "Measurement of adhesion energies and Young's modulus in thin polymer films using a novel axisymmetric peel test geometry," *The European Physical Journal E*, vol. 19, no. 4, pp. 453–459, 2006.

[16] G. Oreski and G. Wallner, "Delamination behaviour of multilayer films for PV encapsulation," *Solar Energy Materials and Solar Cells*, vol. 89, no. 2-3, pp. 139–151, 2005.

[17] M. D. Thouless and H. M. Jensen, "Elastic fracture mechanics of the peel-test geometry," *The Journal of Adhesion*, vol. 38, pp. 3-4, 1992.

[18] M. Farhoodi, S. M. Mousavi, R. Sotudeh-Gharebagh, Z. Emam-Djomeh, A. Oromiehie, and H. Mansour, "A study

on physical aging of semicrystalline Polyethylene terephthalate below the glass transition point," *Journal of Applied Research and Technology*, vol. 10, pp. 698–702, 2012.

[19] X. Centelles, M. Martín, A. Solé, J. Ramon Castro, and L. F. Cabeza, "Tensile test on interlayer materials for laminated glass under diverse ageing conditions and strain rates," *Construction and Building Materials*, vol. 243, Article ID 118230, 2020.

[20] X. Centelles, J. R. Castro, and L. F. Cabeza, "Double-lap shear test on laminated glass specimens under diverse ageing conditions," *Construction and Building Materials*, vol. 249, Article ID 118784, 2020.

[21] F. Ensslen, "Influences of laboratory and natural weathering on the durability of laminated safety glass," *Glass Performance Days*, vol. 2, pp. 584–590, 2007.

[22] K. Machalická and M. Eliášová, "Adhesive joints in glass structures: effects of various materials in the connection, thickness of the adhesive layer, and ageing," *International Journal of Adhesion and Adhesives*, vol. 72, pp. 10–22, 2017.

[23] J. S. Zaroulis and M. C. Boyce, "Temperature, strain rate, and strain state dependence of the evolution in mechanical behaviour and structure of poly(ethylene terephthalate) with finite strain deformation," *Polymer*, vol. 38, no. 6, pp. 1303–1315, 1997.

[24] C. Le Clerc, A. R. Bunsell, and A. Piant, "Influence of temperature on the mechanical behaviour of polyester fibres," *Journal of Materials Science*, vol. 41, pp. 1573–4803, 2006.

[25] A. Arkhireyeva and S. Hashemi, "Effect of temperature on fracture properties of an amorphous poly(ethylene terephthalate) (PET) film," *Journal of Materials Science*, vol. 37, no. 17, pp. 3675–3683, 2002.

[26] Z. Peng, C. Wang, L. Chen, and S. Chen, "Peeling behavior of a viscoelastic thin-film on a rigid substrate," *International Journal of Solids and Structures*, vol. 51, no. 25-26, pp. 4596–4603, 2014.

[27] C. Kovalchick, A. Molinari, and G. Ravichandran, "Rate dependent adhesion energy and nonsteady peeling of inextensible Tapes," *Journal of Applied Mechanics*, vol. 81, no. 4, Article ID 041016, 2013.

[28] ASTM D882-02-standard test method for tensile properties of thin plastic sheeting.

[29] C. Bedon, E. Bergamo, M. Izzi, and S. Noè, "Prototyping and validation of MEMS accelerometers for structural health monitoring—the case study of the pietratagliata cable-stayed bridge," *Journal of Sensor and Actuator Networks*, vol. 7, Article ID 30, 2018.

[30] C. Bedon, "Issues on the vibration analysis of in-service laminated glass structures: analytical, experimental and numerical investigations on delaminated beams," *Applied Sciences*, vol. 9, no. 18, Article ID 3928, 2019.

[31] C. Bedon, M. Fasan, and C. Amadio, "Vibration analysis and dynamic characterization of structural glass elements with different restraints based on operational modal analysis," *Buildings*, vol. 9, no. 1, Article ID 13, 2019.

[32] C. Bedon and S. Noè, "Post-breakage vibration frequency analysis of in-service pedestrian laminated glass modular units," *Vibrations*, vol. 4, no. 4, pp. 836–852, 2021.

[33] K. Kendall, "Thin-film peeling-the elastic term," *Journal of Physics D: Applied Physics*, vol. 8, no. 13, pp. 1449–1452, 1975.

[34] A. J. Kinloch, C. C. Lau, and J. G. Williams, "The peeling of flexible laminates," *International Journal of Fracture*, vol. 66, no. 1, pp. 45–70, 1994.

[35] 3M, "Ultra S800 product technical datasheet-3M™ Scotchshield™ safety & security window film ultra S800 - technical specifications," 2021, https://multimedia.3m.com/mws/media/1511872O/product-bulletin-ultra-s800-window-film.pdf.

[36] Solarcheck, "14 Mil Clear product technical datasheet - safety film," 2021, https://solarcheck.com/it/producto/14-mil-clear/.

[37] Bekaert, "Armorcoat product technical datasheet," 2021, https://www.bekaert.com/.

[38] SMIT, available online: https://smit.atlss.lehigh.edu/?page_id=23.

[39] M. Chang, R. L. Leonard, and S. N. Pakzad, *SMIT User's Guide. Release 1.0*, 2012, https://smit.atlss.lehigh.edu/wp-content/uploads/2012/07/SMIT-Users-Guide.pdf.

[40] M. Chang and S. N. Pakzad, "Observer kalman filter identification for output-only systems using interactive structural modal identification toolsuite," *Journal of Bridge Engineering*, vol. 19, Article ID 04014002, 2014.

[41] ABAQUS computer software, simulia, 2020.

[42] C. Bedon, K. Machalicka, M. Eliasova, and M. Vokac, "Numerical modelling of adhesive connections including cohesive damage," *Challenging Glass Conference Proceedings*, vol. 6, pp. 309–320, 2018.